Characteristics of wall sheath and secondary electron emission under different electron temperatures in a Hall thruster*

Duan Ping(段 萍)[a)†], Qin Hai-Juan(覃海娟)[a)], Zhou Xin-Wei(周新维)[a)], Cao An-Ning(曹安宁)[a)], Chen Long(陈 龙)[b)], and Gao Hong(高 宏)[a)]

[a)] *Department of Physics, Dalian Maritime University, Dalian* 116026, *China*
[b)] *School of Physics and Optoelectronic Technology, Dalian University of Technology, Dalian* 116024, *China*

(Received 4 June 2013; revised manuscript received 23 December 2013; published online 22 May 2014)

In this paper, a two-dimensional physical model is established in a Hall thruster sheath region to investigate the influences of the electron temperature and the propellant on the sheath potential drop and the secondary electron emission in the Hall thruster, by the particle-in-cell (PIC) method. The numerical results show that when the electron temperature is relatively low, the change of sheath potential drop is relatively large, the surface potential maintains a stable value and the stability of the sheath is good. When the electron temperature is relatively high, the surface potential maintains a persistent oscillation, and the stability of the sheath reduces. As the electron temperature increases, the secondary electron emission coefficient on the wall increases. For three kinds of propellants (Ar, Kr, and Xe), as the ion mass increases the sheath potentials and the secondary electron emission coefficients reduce in sequence.

Keywords: Hall thruster, electron temperature, sheath, secondary electron emission

PACS: 52.40.Kh, 52.65.–y **DOI:** 10.1088/1674-1056/23/7/075203

1. Introduction

A Hall thruster is a kind of advanced electric propulsion system, which has been widely used in spacecraft attitude control, station keeping, orbital transfer and some other promoting tasks in space due to its high specific impulse, high thrust power, simple structure, reliable properties and other advantages.[1–5] The XX-9A satellite of China was launched into orbit on 14 October 2012.[6] The plasma in a Hall thruster channel interacts with the wall material (BN), and accordingly forms the un-neutral area which is called the sheath. In the sheath region, the bombardment of high-energy electrons on the solid wall leads to the emission of secondary electrons. The properties of the plasma sheath and the secondary electron emission influence thruster indicators such as efficiency, specific impulse and life.

In 1990, Schwager and Procassini established a PIC (particle-in-cell) method to investigate the influence of the ion temperature on the sheath's properties. A one-dimensional (1D) radial PIC model was employed by Sydorenko to simulate the acceleration region in the sheath in the Hall thruster. Furthermore, Kaganovich and Sydorenko simulated the radial pre-sheath and sheath with a 1D PIC model, and they analyzed the relation between the secondary electron emission and the stability of the sheath.[7–9] By improving the secondary electron emission model which was proposed by Morozov, the Harbin Institute of Technology established a 1D fluid sheath model combined with a two-dimensional (2D) particle sheath model within an insulated wall to study the influence of the electronic anisotropic temperature on the near-wall electron current, as well as the effect of a space–charge-saturated sheath on the near-wall conductivity.[10–13] In addition, the institute established a 1D fluid sheath model, analyzing the influence of the secondary electron emission coefficient on plasma sheath properties in Hall thruster channels numerically.[14–16]

Fluid simulation, hybrid simulation and particle simulation are often used to numerically model the plasma sheath in Hall thrusters. Although the computing efficiency of fluid simulations is higher, electrons are assumed to be in the Maxwell distribution in the fluid model.[17] In actual fact, the electron speed distribution function inside the Hall thruster disobeys the Maxwell distribution.[18,19] Therefore, electron behavior in the sheath region is treated by a 2D particle simulation method in this paper; the potential distribution at the grid nodes and electric field distribution at the particle location are obtained by solving Poisson's equation and kinematic equations. The influences of the electron temperature on the electron density, sheath potential and secondary electron emission coefficient from the wall are investigated; the influences of different propellants on the sheath potential and the secondary electron emission from the wall are also discussed.

*Project supported by the National Natural Science Foundation of China (Grant Nos. 10975026, 11275034, and 11175052), the Key Project of Science and Technology of Liaoning Province, China (Grant No. 2011224007), and the Fundamental Research Funds for the Central Universities of Ministry of Education of China (Grant No. 3132014328).

†Corresponding author. E-mail: duanping591@sohu.com

© 2014 Chinese Physical Society and IOP Publishing Ltd

2. Physical model and boundary conditions

2.1. Physical model

A Hall thruster is a kind of electric propulsion device composed of an inner and outer ceramic sleeve each with a ring structure. Its structure and working principle are shown in Fig. 1.

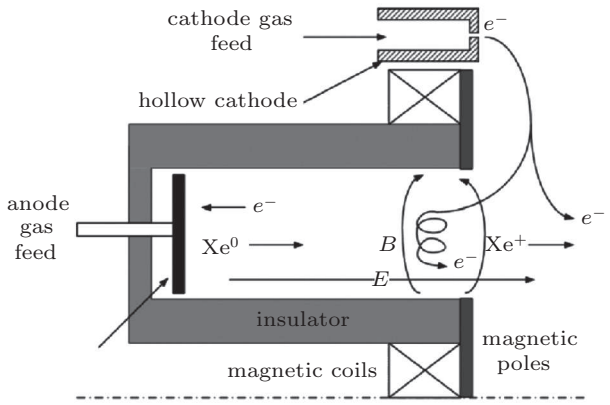


Fig. 1. Structure and working principle of the Hall thruster.

Inside the Hall thruster discharge channel, the magnetic field generated by the plasma self-consistently is much weaker than the external magnetic field, so it can be ignored. In the Hall thruster plasma sheath, the Maxwell equations are as follows:

$$\nabla \cdot \boldsymbol{E} = \frac{\rho}{\varepsilon_0}, \tag{1}$$

$$\nabla \times \boldsymbol{E} = -\frac{1}{c}\frac{\partial \boldsymbol{B}}{\partial t} = 0, \quad \left(\frac{1}{c} = \sqrt{\mu_0 \varepsilon_0}\right), \tag{2}$$

where $\boldsymbol{E}$ is the electric field, $\boldsymbol{B}$ is the magnetic field, μ_0 is the vacuum permeability, ε_0 is the vacuum dielectric constant, and ρ is the electric charge density. The electric field can be given as

$$\boldsymbol{E} = -\nabla \phi. \tag{3}$$

By introducing Eq. (3) into Eq. (1), the Poisson equation is written as

$$\nabla^2 \phi = -4\pi\rho. \tag{4}$$

The numerical simulation region is shown in Fig. 2. In the column coordinate system the 2D Poisson equation can be written as follows:

$$\frac{1}{r}\frac{\partial}{\partial r}\left(r\frac{\partial \phi}{\partial r}\right) + \frac{\partial^2 \phi}{\partial^2 z} = -\frac{e}{\varepsilon_0}(n_\mathrm{i} - n_\mathrm{e}), \tag{5}$$

where ϕ is the potential, n_i is the ion density and n_e is the electron density, e is the unit of charge. The grid is divided by identical mesh spaces along the axial and radial directions. Applying the central difference method to Eq. (5) yields

$$\frac{1}{r}\frac{\phi_{i,j+1} - \phi_{i,j-1}}{2\Delta r} + \frac{\phi_{i,j+1} - 2\phi_{i,j} + \phi_{i,j-1}}{(\Delta r)^2} + \frac{\phi_{i+1,j} - 2\phi_{i,j} + \phi_{i-1,j}}{(\Delta z)^2} = -\frac{e}{\varepsilon_0}(n_\mathrm{i} - n_\mathrm{e})_{i,j}. \tag{6}$$

Equation (6) can be simplified to

$$\frac{(\Delta r)^2}{(\Delta z)^2}(\phi_{\mathrm{i}+1,\mathrm{j}} + \phi_{\mathrm{i}-1,\mathrm{j}}) - 2\left[1 + \frac{(\Delta r)^2}{(\Delta z)^2}\right]\phi_{i,j} + \left(\frac{r_{i,j+1/2}}{r_{i,j}}\phi_{i,j+1} + \frac{r_{i,j-1/2}}{r_{i,j}}\phi_{i,j-1}\right) = -\frac{e}{\varepsilon_0}(n_\mathrm{i} - n_\mathrm{e})_{i,j}(\Delta r)^2. \tag{7}$$

For the movement of a single particle in the case with an electromagnetic field, the kinematic equations are as follows:

$$\frac{\mathrm{d}}{\mathrm{d}t} m\boldsymbol{v} = q(\boldsymbol{E} + \boldsymbol{v} \times \boldsymbol{B}), \tag{8}$$

$$\frac{\mathrm{d}}{\mathrm{d}t} x = \boldsymbol{v}, \tag{9}$$

where m is the mass of the charged particle, $\boldsymbol{v}$ is the velocity and x is the position. The Boris algorithm, which has second-order accuracy, is employed

$$\boldsymbol{v}^- = \boldsymbol{v}^{t-\Delta t/2} + e\Delta t \boldsymbol{E}^t/2m, \tag{10}$$

$$\boldsymbol{v}' = \boldsymbol{v}^- + \boldsymbol{v}^- \times \boldsymbol{t}^t, \tag{11}$$

$$\boldsymbol{v}^+ = \boldsymbol{v}^- + \boldsymbol{v}' \times 2\boldsymbol{t}^t/(1 + \boldsymbol{t}^t \times \boldsymbol{t}^t), \tag{12}$$

$$\boldsymbol{v}^{t+\Delta t/2} = \boldsymbol{v}^+ + e\Delta t \boldsymbol{E}^t/2m, \tag{13}$$

where $\boldsymbol{t}^t = e\Delta t \boldsymbol{B}^t/2m$ and t is the superscript representing the moment.

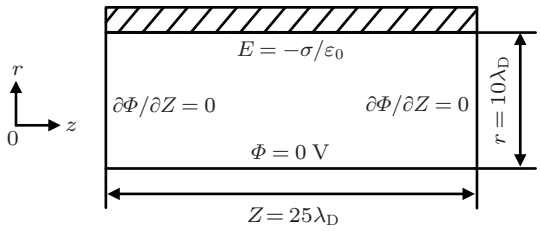


Fig. 2. Simulation region and boundary conditions.

2.2. Boundary conditions

The simulation region is $z = 25\lambda_\mathrm{D}$ in the axial direction and $r = 10\lambda_\mathrm{D}$ in the radial direction. The mesh space is $\Delta z = \Delta r = 0.5\lambda_\mathrm{D}$ and the time step is $\Delta t = 0.1\omega_\mathrm{p}^{-1}$, where λ_D is the Debye length, ω_p is the plasma frequency. In the simulation, the electron density is $n_\mathrm{e} = 10^{18}$ m^{-3}, and the magnetic field is $B = 0.02$ T. According to the formula $r_\mathrm{c} = m_\mathrm{e}v_\mathrm{e}/eB$, the electron Larmor radius length ($r_\mathrm{c} \approx 0.5$ mm) is larger than the radial length of the simulation region ($r \approx 0.3$ mm), so the electron is assumed to be un-magnetized. Since the ions are heavier than the electrons, and the ion response speed is lower, the ion density and speed are assumed to be constant in the simulation region, which are taken as the background particle, and enter with Bohm speed.

In the calculation, the quasi-neutral condition is adopted at the sheath boundary. In the quasi-neutral region ($r = r_0 \sim 3\lambda_D$), electrons are arranged uniformly and the electronic speed obeys the Maxwell distribution at each time step.[20] When a particle moves to the simulation boundary, it is considered to be disappearing, and the corresponding information of this particle is deleted. The periodic boundary condition is applied to the right and left sides of the simulation region. Electrons collide with the insulated wall (BN), which will cause secondary electron emission. When an electron hits the wall, one of the following four events may occur:[21–23] the electron is absorbed by the wall, the electron is reflected elastically, the electron knocks out one electron or the electron knocks out two electrons. The corresponding probabilities of the four events are respectively

$$W_0(\varepsilon) = 0.5\exp\left(-\frac{\varepsilon^2}{43.4592^2}\right), \tag{14}$$

$$W_r(\varepsilon) = 0.5\exp\left(-\frac{\varepsilon^2}{30^2}\right), \tag{15}$$

$$W_2(\varepsilon) = 1-\exp\left(-\frac{\varepsilon^2}{127.8958^2}\right), \tag{16}$$

$$W_1(\varepsilon) = 1 - W_0(\varepsilon) - W_r(\varepsilon) - W_2(\varepsilon), \tag{17}$$

where ε is the energy of the entering electron. For the insulated wall boundary, there is energy loss both when the electron knocks out secondary electrons and when electrons collide with the wall inelastically. The electron energy is assumed to obey the Maxwell distribution. At the sheath boundary, the potential is set to zero. According to the periodic boundary, the potential satisfies $\partial\Phi/\partial z = 0$. The potential boundary condition is given by $\boldsymbol{E} = -\sigma/\varepsilon_0$ at the insulated wall boundary, where σ is the surface charge density. In the particle cloud model, although the plasma parameters of the simulation system are much smaller than the plasma parameters of the real physical system, the collision frequency is still small, and the collisionless condition can be satisfied. Therefore, only the collisions between electrons and the wall are considered in the simulation region.[24]

3. Results and discussion

3.1. Electron temperature effect on the sheath properties

Figure 3 shows the evolutions of electron density as a function of electron temperature. When the electron temperature is relatively low, the electron density in the sheath declines exponentially, and the electron density on the wall is one order of magnitude lower than within the sheath. When the electron temperature is relatively high, electron density is almost constant in the sheath, but it increases rapidly in the region near the wall, and the magnitude is about 1.5 to 3.5 times higher. This is because when the electron temperature is relatively high, slow electrons within the sheath can pass through the high potential barrier of the sheath and arrive at the wall, generating more secondary electrons. Besides sheath potential drop is small which reduces the speed of the secondary electrons. Therefore a large number of secondary electrons are kept in the region near the wall, so the electron density increases rapidly near the wall.

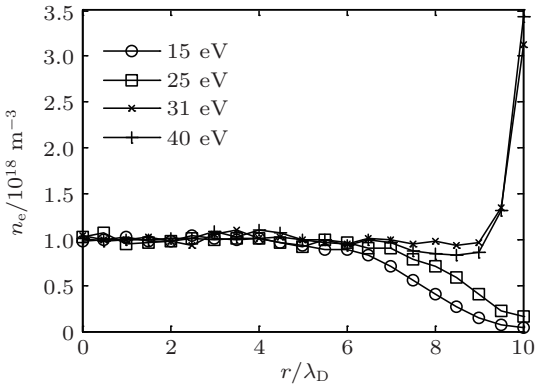


Fig. 3. Variations of electron density n_e with r/λ_D at different electron temperatures ($z/\lambda_D = 12.5$).

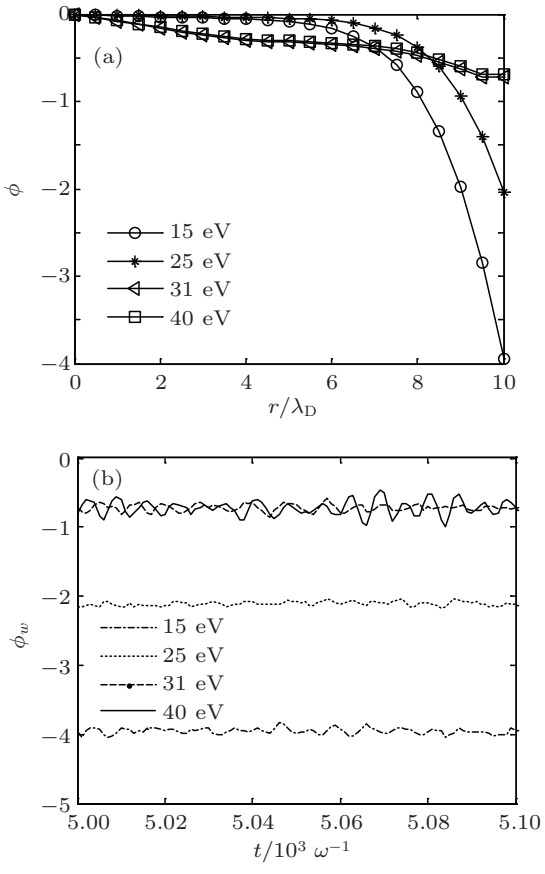


Fig. 4. (a) Variations of sheath potential with r/λ_D at different electron temperatures ($z/\lambda_D = 12.5$) and (b) variations of the surface potential with time at different electron temperatures ($z/\lambda_D = 12.5$).

Figure 4 shows the influences of electron temperature on the sheath potential and the surface potential. From Fig. 4 it is clear that the sheath potential decreases along the radial direction, and when the electron temperature is relatively high ($T_e = 31$ eV, 40 eV), the surface potential is much higher than

when the electron temperature is low ($T_e = 15$ eV, 25 eV). This is because when the electron temperature is relatively high, the electron density near the wall is higher than within the sheath. On the other hand, when the electron temperature is relatively low, the electron density near the wall is lower than within the sheath. The incident electrons neutralize with the ions at the wall, which reduces the ion density on the wall. Therefore, when the electron temperature is low, the ion density on the wall is higher than when the electron temperature is high. Therefore, the surface potential in the case with low electron temperature is lower than in the case with high electron temperature. It can be seen from Fig. 4(b), when the electron temperature is relatively high, the oscillation of the surface potential with time is more obvious than when electron temperature is low; when the electron temperature is relatively high, the perturbation of the sheath boundary is obvious, and the damping of sheath is small, so the sheath potential maintains a continuous oscillation. When the electron temperature is relatively low, the electron motion is relatively slow, the perturbation of the sheath boundary is small, and the sheath damping is large, therefore the sheath potential maintains an approximately stable value.

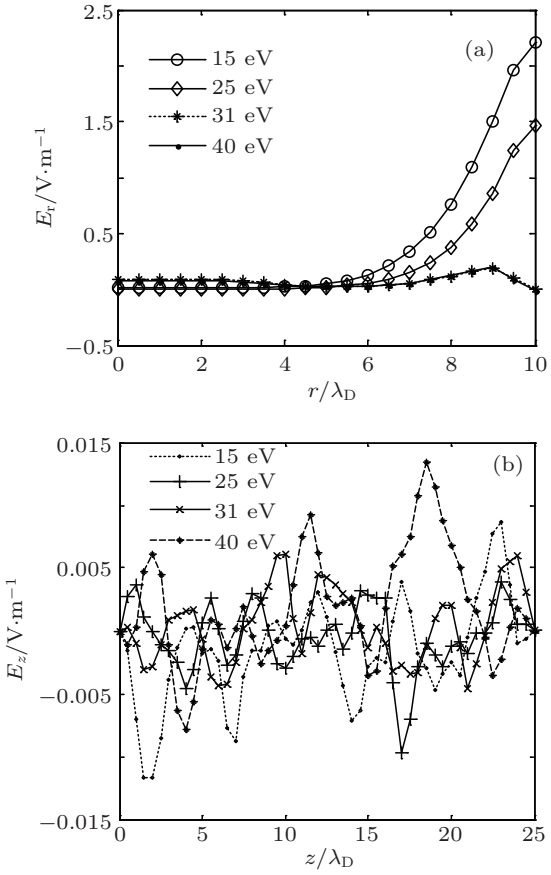


Fig. 5. (a) Distributions of the radial electric field at different electron temperatures and (b) variations of axial electric field with z/λ_D at different electron temperatures.

Figures 5(a) and 5(b) show the influences of the electron temperature on the radial and axial electric fields within the sheath, respectively. It can be seen that when the electron temperature is low, the variation of the radial electric field is more obvious than when the electron temperature is high. The sheath potential drop at low electron temperature is higher than at high electron temperature. According to $\boldsymbol{E} = -\nabla\varphi$, the sheath radial electric field increases with the increase of sheath potential drop. It can be seen from Fig. 5(b) that, the influence of the electron temperature on the axial field is relatively small, and the variation is of the order of 10^{-3}. Since electrons move approximately along the radial direction in the sheath, the electron temperature within the sheath has little effect on the axial electric field.

3.2. Electron temperature effect on the secondary electron emission coefficient

Figures 6(a) and 6(b) show the influences of the electron temperature on the density of electrons hitting the wall and the density of secondary electrons emitted from the wall, respectively. It can be seen that with the increase of electron temperature, both the density of electrons hitting the wall and the density of secondary electrons emitted from the wall increase. As the electron temperature increases, a large number of slow electrons pass through the high potential barrier of the sheath and reach the wall, which causes the increase

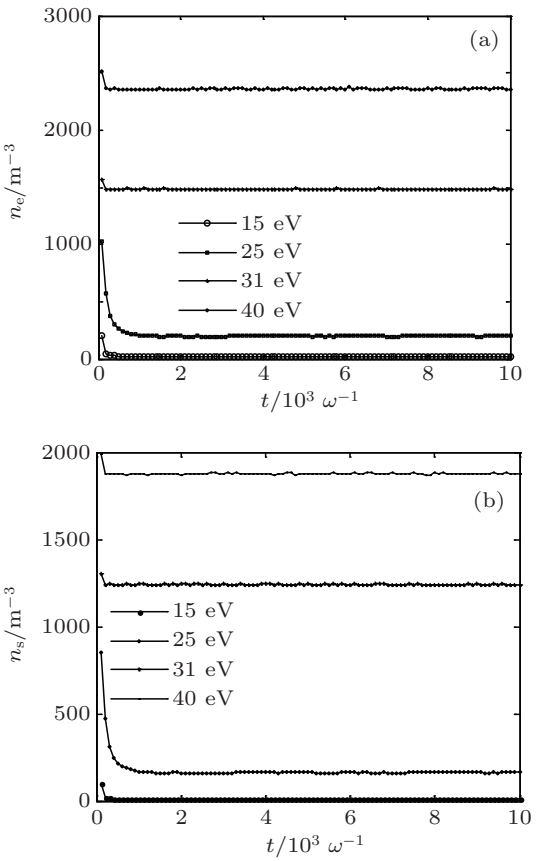


Fig. 6. (a) Variations of the density of electrons hitting the wall with time at different electron temperatures and (b) variations of the density of secondary electrons emitted from the wall with time at different electron temperatures.

of electron energy at the wall. Therefore, when the electron temperature is relatively high, the number of secondary electrons emitted from the wall increases. Figure 7 shows the relation between the electron temperature and the secondary electron emission coefficient. It can be seen that as the electron temperature increases, the secondary electron emission coefficient increases. This is because as the electron temperature increases, the electron energy near the wall increases, which leads to the increase in the probability of the emission of secondary electrons.

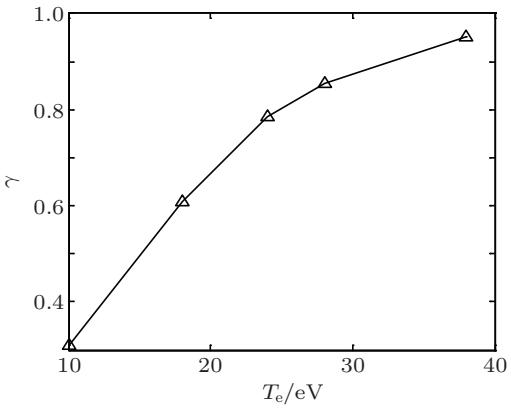


Fig. 7. Dependence of the secondary electron emission coefficient on electron temperature.

3.3. Different propellant effects on sheath properties

Figures 8 and 9 show the sheath potential and the secondary electron emission coefficient with different propellants, respectively. It can be seen that, for three kinds of propellants (Ar, Kr, Xe), the sheath potential drops increase in sequence, and meanwhile the secondary electron emission coefficients decrease. As is well known, the sheath potential can be calculated from[25]

$$\frac{e\Phi}{T_e} = -\ln\left[(1-\gamma)\left(\frac{M}{2\pi m}\right)^{1/2}\right], \tag{18}$$

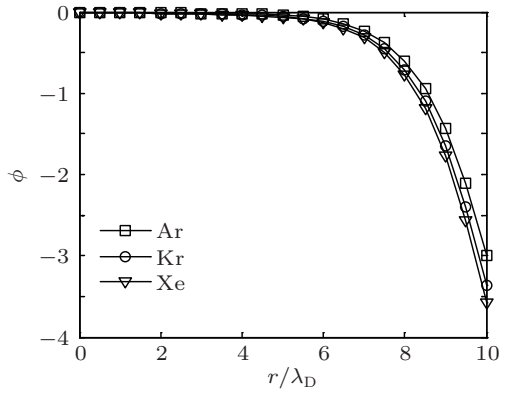


Fig. 8. Variations of sheath potential with r/λ_D for three different kinds of propellants ($z/\lambda_D = 12.5$).

where γ is the secondary electron emission coefficient, M is the ion mass and m is the electron mass. For three kinds of propellants (Ar, Kr, Xe), as the ion mass values increase in sequence, the sheath potential drop increases, which increases the electron energy loss when it passes through the sheath. According to formula (18), the secondary electron emission coefficient of the wall decreases.

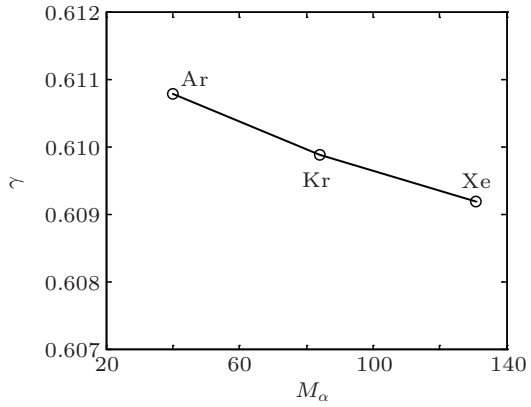


Fig. 9. Variations of secondary electron emission coefficient with propellant ion mass for three different kinds of propellants.

4. Conclusions

In this paper, we numerically investigate the influences of the electron temperature and propellant type on the stability of the sheath in a Hall thruster channel by using the PIC simulation method. The numerical results show that when the electron temperature is relatively low (T_e = 15 eV, 25 eV), the electron density within the sheath decreases along the radial direction towards the wall, and its minimal value appears near the wall; the sheath is stable; moreover, the sheath potential drop and the radial electric field are both large. When the electron temperature is high (T_e = 31 eV, 40 eV), a lot of slow electrons can pass through the high potential barrier of the sheath and reach the wall, so the electron density near the wall increases rapidly; however, the electron density in most of the region within the sheath remains the same, the sheath maintains amplitude oscillation and the stability of the sheath reduces. For three kinds of propellants (Ar, Kr, Xe), the sheath potentials and the secondary electron emission coefficients reduce in sequence; the capabilities of sheath shielding plasma are enhanced in sequence; and the collision between the particles and the wall become weaker also in sequence, which reduces the corrosion effect caused by the particles colliding with the wall. Therefore, Xe is usually used as thruster propellant.

References

[1] Qiu G, Kang X L, Qiao C X and Feng Y 2012 *J. Rocket Propulsion* **38** 1667 (in Chinese)
[2] Mao G W, Fu X P and Chen M L 2008 *Mech. Sci. Tech. Aero. Eng.* **27** 853 (in Chinese)

[3] Steven R O and John M S 2001 3*rd International Spacecraft Propulsion Conference*, October 10–13, 2000, Cannes, France, p. 717
[4] Henry W B, Mark J O, Jones P A and Cassady R J 2002 *Acta Astronautica* **51** 57
[5] Jankovsky R S, Jacobson D T, Sarmiento C J, Pinero L R, Manzella D H, Man H R R and Peterson P Y 2002 38*th Joint Propulsion Conference and Exhibit*, July 7–10, 2002, Indianapolis, Indiana, p.3675
[6] Kang X L, Yu S L, Qiao C X, Zhao Z, Hang G R, Qiu G, Chen H B and Zhang Y 2012 *Proceeding of the* 8*th Chinese Electric Propulsion Conference*, November 2012, p. 180 (in Chinese)
[7] Sydorenko D, Smolyakov A, Kaganovich I and Raitses Y 2006 *IEEE Trans. Plasma Sci.* **34** 815
[8] Sydorenko D, Smolyakov A, Kaganovich I and Raitses Y 2008 *Phys. Plasmas* **15** 053506
[9] Kaganovich I D, Raitses Y, Sydorenko D and Smolyakov A 2007 *Phys. Plasmas* **14** 057104
[10] Zhang F K 2009 *Study on Dynamic Characteristics of Dielectric Wall Sheath and its Effect on near Wall Conductivity in Hall Thrusters* (Ph.D. Thesis) (Harbin: Harbin Institute of Technology of China) (in Chinese)
[11] Zhang F K, Ding Y J, Qing S W and Wu X D 2011 *Chin. Phys. B* **20** 125201
[12] Zhang F K, Ding Y J, Li H, Wu X D and Yu D R 2011 *Phys. Plasmas* **18** 103512
[13] Yu D R, Qing S W, Wang X G, Ding Y J and Duan P 2013 *Acta Phys. Sin.* **62** 055202 (in Chinese)
[14] Duan P, Li X, E P and Qing S W 2011 *Acta Phys. Sin.* **60** 125203 (in Chinese)
[15] Duan P, Shen H J, Liu J Y, Li X, E P and Chen L 2011 *J. Propulsion Technology* **31** 185 (in Chinese)
[16] Duan P, Li X, Shen H J, Chen L and E P 2012 *Plasmas Sci. Technol.***14** 1
[17] Zhao J, Tang D L and Wang L S 2008 *Aero. Shanghai* **2** 36 (in Chinese)
[18] Bugrova A I, Desyatskov A V and Morozov A I 1992 *Phys. Plasmas* **18** 501
[19] Guerrini G, Michaut C, Dudeck M, Vesselovzorov A N and Bacal M 1997 25*th International Electric Propulsion Conference*, August 24–28, 1997, Cleveland, Ohiop, American, p. 326
[20] Yu D R, Zhang F K, Li H and Liu H 2009 *Acta Phys. Sin.* **58** 1844 (in Chinese)
[21] Dunaevsky A, Raitses Y and Fisch N J 2003 *Phys. Plasmas* **10** 2574
[22] Barral S, Makowski K, Peradzyński Z, Gascon N and Dudeck M 2003 *Phys. Plasmas* **10** 4137
[23] Shu S 2006 *The Influence of Secondary Electron Emission on the Sheath and Near Wall Conductivity in Stationary Plasma Thruster* (MS Thesis) (Harbin: Harbin Institute of Technology of China) (in Chinese)
[24] Fu Z F and Hu Y Q 1995 *Space Plasma Numerical Simulation* (3rd edn.) (Heifei: Anhui Science & Technology Publishing House) (in Chinese)
[25] Sydorenko D 2006 *Particle-in-Cell Simulations of Electron Dynamics in Low Pressure Discharges with Magnetic Fields* (Ph.D. Thesis) (Saskatchewan: University of Saskatchewan)